Proteome-Wide Analysis of Cysteine Reactivity during Effector-Triggered Immunity[1][OPEN]

Evan W. McConnell,[a,2] Philip Berg,[b,2] Timothy J. Westlake,[c,2] Katherine M. Wilson,[a] George V. Popescu,[d,e] Leslie M. Hicks,[a,3] and Sorina C. Popescu[b,3,4]

[a]Department of Chemistry, the University of North Carolina at Chapel Hill, Chapel Hill, North Carolina 27514
[b]Department of Biochemistry, Molecular Biology, Entomology, and Plant Pathology, Mississippi State University, Mississippi State, Mississippi 39762
[c]Department of Plant Pathology and Plant-Microbe Biology, Cornell University, Ithaca, New York 14850
[d]Institute for Genomics, Biocomputing and Biotechnology, Mississippi State University, Mississippi State, Mississippi 39762
[e]The National Institute for Laser, Plasma & Radiation Physics, 077126 Măgurele, Ilfov, Romania

ORCID IDs: 0000-0002-2295-3027 (E.W.M.); 0000-0001-5780-8252 (S.C.P.).

A surge in the accumulation of oxidants generates shifts in the cellular redox potential during early stages of plant infection with pathogens and activation of effector-triggered immunity (ETI). The redoxome, defined as the proteome-wide oxidative modifications of proteins caused by oxidants, has a well-known impact on stress responses in metazoans. However, the identity of proteins and the residues sensitive to oxidation during the plant immune response remain largely unknown. Previous studies of the thimet oligopeptidases TOP1 and TOP2 placed them in the salicylic acid dependent branch of ETI, with a current model wherein TOPs sustain interconnected organellar and cytosolic pathways that modulate the oxidative burst and development of cell death. Herein, we characterized the ETI redoxomes in Arabidopsis (*Arabidopsis thaliana*) wild-type Col-0 and *top1top2* mutant plants using a differential alkylation-based enrichment technique coupled with label-free mass spectrometry-based quantification. We identified cysteines sensitive to oxidation in a wide range of protein families at multiple time points after pathogen infection. Differences were detected between Col-0 and *top1top2* redoxomes regarding the identity and number of oxidized cysteines, and the amplitude of time-dependent fluctuations in protein oxidation. Our results support a determining role for TOPs in maintaining the proper level and dynamics of proteome oxidation during ETI. This study significantly expands the repertoire of oxidation-sensitive plant proteins and can guide future mechanistic studies.

Plant stress is responsible for most crop yield loss and is also one of the greatest challenges to overcome in modern agriculture (Dubé et al., 2012). It is critical to understand how plants sense and integrate diverse stress signals to elicit physiological responses for survival and, in the long-term, to reach a predictive understanding of the adaptation and tolerance mechanisms.

Under normal physiological conditions, reactive oxygen species (ROS) produced in various cellular compartments such as chloroplasts and mitochondria, are essential to the plant growth and development; cellular ROS concentration is maintained at low levels due to the tight regulation of their production and degradation through enzymatic and nonenzymatic processes (Noctor and Foyer, 2016). Infection with pathogens perturbs ROS homeostasis and lead to oxidant accumulation at above-physiological levels followed by localized shifts in the reduction-oxidation (redox) potential of the apoplast, cytosol, and intracellular compartments (Suzuki et al., 2012; Han et al., 2013). Cellular oxidants have a strong impact on the proteome, whereby reactive protein cysteines are oxidized—a process well documented in metazoans (Yang et al., 2016), and in the initial stages of being evaluated and understood in plants (Akter et al., 2015b). Under physiological conditions or stress Cys thiols (R-SH) may deprotonate to reactive thiolates ($R\text{-}S^-$) and become modified by ROS to reversibly oxidized products such as sulfenic acid (R-SOH) and disulfides (R-SS-R′). Further oxidation of sulfenic acids may lead to irreversible products such as sulfinic acid

[1]This work was supported by the National Science Foundation (NSF-MCB grant no. 1714157 to S.C.P. and NSF-MCB grant no. 1714405 to L.M.H.).

[2]These authors contributed equally.

[3]Senior author.

[4]Author for contact: scp319@msstate.edu.

The author responsible for distribution of materials integral to the findings presented in this article in accordance with the policy described in the Instructions for Authors (www.plantphysiol.org) is: Sorina C. Popescu (scp319@msstate.edu).

T.J.W. grew plants, performed all plant assays, and collected the plant material; E.W.M. and K.M.W. processed the plant material, performed LC-MS/MS analysis, and preprocessed the data; P.B. implemented the statistical data analysis pipeline and contributed to data mining; P.B. and G.V.P. performed the statistical analysis of data; S.C.P. performed the mining and functional analysis of the data, and wrote the manuscript; G.V.P., E.W.M., L.M.H., and P.B. edited and contributed to the writing.

[OPEN]Articles can be viewed without a subscription.
www.plantphysiol.org/cgi/doi/10.1104/pp.18.01194

(R-SO_2H) and sulfonic acid (R-SO_3H). Following oxidation of Cys residues, a protein's functional and structural characteristics can change significantly; thus, ROS-mediated modification of cysteines provides an important protein post-translational regulatory mechanism. It is considered that ROS-sensing mechanisms and signal transduction rely on such oxidative modifications of redox sensor proteins (Noctor and Foyer, 2016).

The study of oxidant agents and their effects on proteins in the context of plant interactions with pests and pathogens has identified proteins that act as sensors and enhanced our understanding of redox signaling and the molecular mechanisms driving it (Spoel and Loake, 2011). Plant infection with avirulent pathogens triggers the synthesis of salicylic acid (SA) and strong localized oxidative bursts in multiple cellular compartments—events considered central to the plant immune response (Mou et al., 2003). A positive feedback loop between SA and ROS synthesis is maintained until a threshold is reached for the activation of SA signaling and the effector-triggered immunity (ETI; Rustérucci et al., 2001). Several components in the SA-mediated pathways are regulated by changes in the cellular redox homeostasis (Couturier et al., 2013). Investigations from our and other groups of two Arabidopsis (*Arabidopsis thaliana*) thimet oligopeptidases—the organellar TOP1 and cytosolic TOP2—revealed their roles as participants in redox processes and as likely subjects of redox regulation in the context of the ETI and chloroplast-originating oxidative stress (Polge et al., 2009; Kmiec et al., 2013; Moreau et al., 2013; Westlake et al., 2015). Both oligopeptidases are required for plant defense to avirulent strains of *Pseudomonas syringae* through the activation of the resistance proteins RPS2 or RPS4, and necessary to regulate the programmed cell death (PCD). In a current model, TOPs sustain interconnected organelle and cytosol proteolytic pathways that regulate the ETI oxidative burst and plant resistance to pathogens (Kmiec et al., 2013; Westlake et al., 2015).

Mass spectrometry has a great potential to allow the systematic exploration of the plant redoxome. Several recent studies report proteome-wide mining of hydrogen peroxide (H_2O_2)-sensitive cysteines in several plant species (Alvarez et al., 2011; Wang et al., 2012b; Muthuramalingam et al., 2013; Liu et al., 2014; Slade et al., 2015), and collectively, highlight the broad impacts of ROS on plant proteomes. However, the composition of the plant redoxome in response to plant-produced ROS, the identity of redox sensors, and their contribution to plant defense and adaptive pathways remain largely unknown. Mass spectrometry-based methodologies are needed to permit the quantitative and site-specific mapping of redox-mediated modification of protein amino acid residues. Moreover, applying proteome-wide mining to biological material undergoing physiologically relevant oxidative stress responses would help to determine the biological functions of thiol sensitivity in particular proteins or cellular pathways.

In this study, we enriched proteins with oxidative post-translational modification (oxPTM) for the identification and quantification of reversible Cys oxidation in the Arabidopsis proteome and characterized the thiol redoxomes of Col-0 wild-type and the *top1top2* null mutant plants at the early stages of the ETI response.

RESULTS

Strategy for Quantitative Profiling of Reversible Cys Oxidation in Plants Undergoing the Effector-Triggered Immune Response

We have developed a strategy to study changes in protein Cys oxidation occurring during the ETI "oxidative burst" (Fig. 1A). The null mutant *top1top2* is known to be more susceptible than the wild-type Col-0 to the bacterial pathogen *P. syringae* DC3000 pv. *tomato* (*Pst*) carrying the avirulence gene avrRpt2 (Moreau et al., 2013). To assess the cellular redox stress and the progression of the hypersensitive response (HR) cell death in *top1top2*, we quantified ion leakage in leaf tissue of plants inoculated with *Pst* avrRpt2 (Fig. 1B). Infiltration of *Pst* avrRpt2 at high inoculum density (10^6 CFU/mL) into leaves of Col-0 produced maximum conductivity values at 8 h postinoculation (hpi), which were sustained at 12 hpi, as previously shown (Katagiri et al., 2002). By comparison, *top1top2* plants had significantly reduced levels of ion leakage at 8 hpi and increased levels at 12 hpi. The results suggest a defect in the progression of the ETI oxidative burst in *top1top2*. No discernable increase in conductivity was recorded in the *rps2* control, or any of the genotypes analyzed when infiltrated with $MgCl_2$ (Supplemental Fig. S1A). Next, to characterize the protein oxidation events triggered by the ETI oxidative burst and gain insight into the probable causes of *top1top2* susceptibility, we inoculated Col-0 and *top1top2* with *Pst* avrRpt2 (10^5 CFU/mL), the condition under which the difference in pathogen growth between Col-0 and *top1top2* was found as statistically significant (Moreau et al., 2013). The pathogen- and mock (buffer)-inoculated leaf tissue was collected for processing and mass spectrometry analysis at 8 hpi and 12 hpi in biological triplicates.

Successful redox proteomics experiments are founded on the steps taken to preserve the in vivo thiol status of cellular proteins. During cell lysis and sample preparation, redox-active enzymes and artificial oxidation can perturb thiol-disulfide equilibria and lead to misinterpretation of results (Hansen and Winther, 2009). To address this issue, free thiols were blocked by iodoacetamide (IAM), an irreversible alkylating agent, under denaturing conditions during cellular lysis to prevent artificial oxidation of in vivo reduced cysteines (Fig. 1C). Blocked proteins were reduced using dithiothreitol (DTT) before buffer exchange for the removal of the excess reducing agent. Nascent protein thiols, formerly in vivo reversibly oxidized cysteines, were then covalently bound to the Thiopropyl Sepharose 6B (TPS6B) resin by a thiol-disulfide exchange reaction.

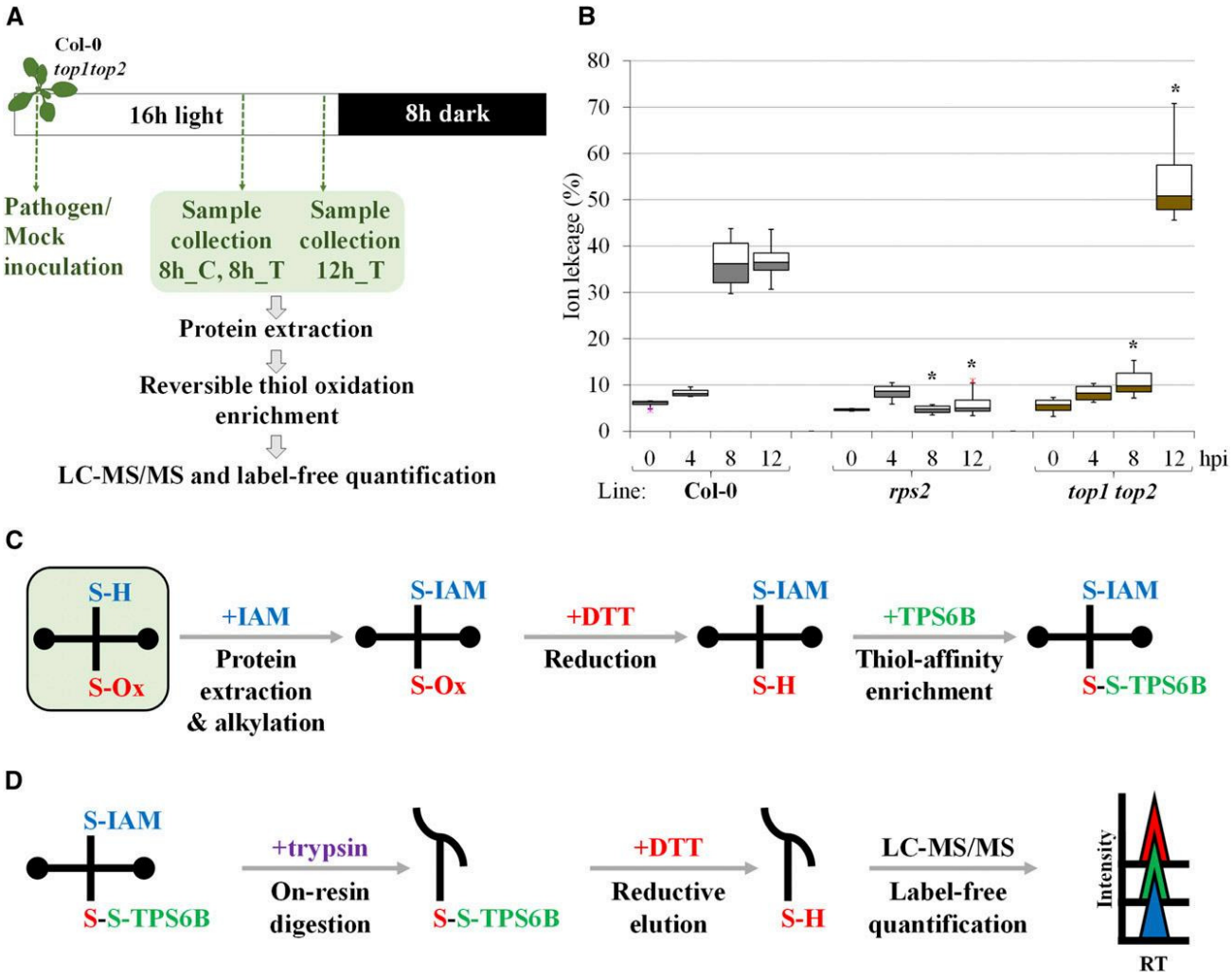

Figure 1. Label-free quantitative analysis of the in vivo oxidation status of the Arabidopsis proteome. A, Diagram of the experimental strategy used in this study. For the determination of the in vivo oxidation status of Cys residues in the Arabidopsis proteome, plants grown under long-day conditions (16 h light/8 h dark) were inoculated with buffer-only (Mock) or with *Pst* avrRpt2 and tissue samples were collected at 8 hpi and 12 hpi. Following protein extraction, peptides with reversible redox modifications at cysteines were enriched (as described in C), and peptides were identified based on fragment ions detected in LC-MS/MS. B, Development of the HR in Arabidopsis plants undergoing the effector-triggered immune response. Various plant genotypes (Col-0, *rps2*, and *top1top2*) were inoculated with *Pst* avrRpt2 and development of cell death during the HR was monitored by measuring the electrolyte leakage from inoculated tissue at multiple time points (hpi). Asterisk (*) represents significant differences ($P < 0.01$) in comparison to that in Col-0 at each respective time point (Student's *t* test parameters: two-tailed distribution, two-sample unequal variance). Four replicates were analyzed for each infiltration group per time point per line. C, Workflow for the protein-level enrichment of reversible Cys oxidation. Free thiols were blocked by IAM during cell lysis. Blocked proteins were reduced, and nascent protein thiols were then covalently bound to the TPS6B resin. D, Workflow for processing Cys-bound redox proteins for LC-MS/MS analysis. Enriched Cys-peptides were eluted from the resin using DTT, analyzed via LC-MS/MS, and processed through an informatics pipeline for site-specific, global profiling of the reversibly oxidized proteome. RT, retention time.

To ensure complete alkylation, we incubated blocked proteins with TPS6B resin before DTT reduction to bind any left-over reduced Cys and analyzed the proteins by SDS-PAGE (Supplemental Fig. S1B). This negative control was observed to have appreciably low background, especially compared to samples reduced with DTT before enrichment, thereby demonstrating efficient alkylation of in vivo reduced Cys. Proteins bound were on-resin digested with trypsin, and enriched Cys-peptides were eluted using DTT and analyzed via liquid chromatography–mass spectrometry (LC-MS/MS; Fig. 1D).

The ETI-Triggered Reversible Cys Redoxomes of Col-0 and top1top2

LC-MS/MS data were processed through a statistical pipeline for label-free site-specific global profiling of the

reversibly oxidized proteome (Supplemental Fig. S2A). The data analysis pipeline consists of: (1) data normalization and variance-stabilization, (2) data filtering, (3) missing data imputation, (4) linear model analysis (*limma*), (5) differential analysis using *limma* output and fold change criteria, (6) multiple imputation and binomial testing, (7) time-series clustering analysis, (8) structure-reactivity clustering analysis of Cys residues, and (9) functional Gene Ontology (GO) annotation analysis. The first peptide analysis steps follow the implementation of the peptide-centric proteomics pipeline described in Berg et al. (2019), which has demonstrated very good performance for analysis of reversible oxidized cysteines on a benchmark dataset. An important result from our previous study was the significant performance improvement obtained when using a linear model in combination with multiple data imputations for comparative analysis of large-scale reversible Cys oxidation datasets. For missing values, we performed 100 multiple imputations generating 100 unique datasets. Data imputation was performed by sampling values from a normal distribution with parameters robustly estimated from the entire dataset. We use the *limma* method (Ritchie et al., 2015) with a significance threshold of 0.05 and a log fold change of ±1 to identify differentially oxidized cysteines together with multiple imputations to decide on statistically significant changes in proteome quantitation due to missing data (Supplemental Table S1). Comparisons among data sets were performed at 8 hpi and 12 hpi with the pathogen for the two genotypes under treatment (T) or control conditions (C), to detect changes in Cys oxidation. Pearson correlation was calculated for each unique combination of samples (Supplemental Fig. S2B) demonstrating the high reproducibility of the label-free quantitation (LFQ) methodology across biological replicates. Each comparison distinguished oxidized Cys-sites with significantly changing abundance (i.e. the proportion of proteins bearing a particular Cys becoming reduced or oxidized with decreasing or increasing abundance, respectively).

We detected significant changes in Cys oxidation between and within genotypes. Oxidized cysteines relative abundance spanned six orders of magnitude, demonstrating a wide range in the level of oxidation of individual residues within the proteome and the sensitivity of LFQ. Overall, in Col-0, we identified 2,113 oxidation-sensitive sites and mapped them to 913 Universal Protein Resource (UniProt) identifiers; for *top1top2*, 1,942 oxidation-sensitive sites were mapped to 823 UniProt identifiers; 338 peptides mapping to 226 proteins had significantly changed abundance in *top1-top2* (Fig. 2A). Col-0 and *top1top2* were most similar at 12 hpi as shown by both Cys- and protein-centric analyses; the largest differences were calculated for 8h-C versus 8-hpi and 8h-C versus 12-hpi sets (Supplemental Fig. S2, C and D). Further analysis compared the proportion of the not-significant cysteines (first bars in Supplemental Fig. S2, C and D) to the 10 biggest sets of significant cysteines (bars 2–11 in

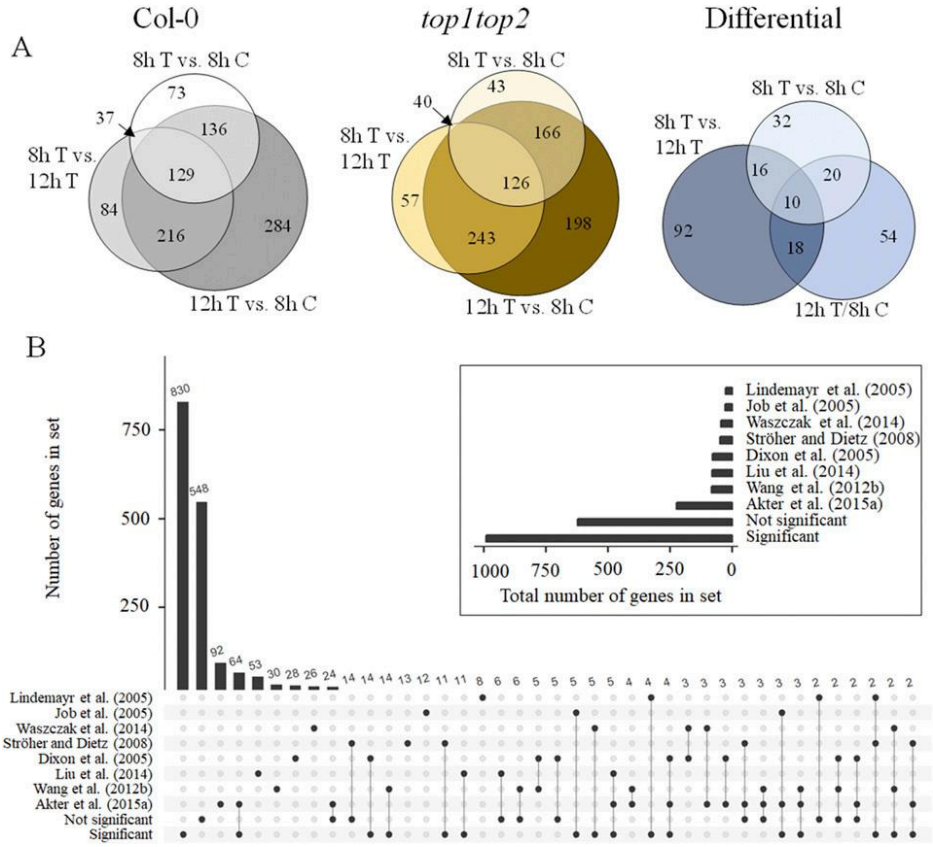

Figure 2. Col-0 and *top1top2* Cys redoxomes. A, Venn diagrams representing the overlap of peptides with experimentally identified sensitive cysteines in Col-0 and *top1top2* plants undergoing the effector-triggered immune response, and oxidized peptides with statistically significant differential accumulation ("Differential") in controls and after inoculation with the pathogen. The numbers represent numbers of peptides with potentially sensitive Cys residues. B, Comparative analysis of oxidation-sensitive proteins from this study with published sets. The bar plot shows the 40 largest sets (*x* axis) containing common genes unique to the selected datasets (*y* axis) represented as shaded (black) dots. The inset bar plot shows the total number of proteins identified in each study.

Supplemental Fig. S2, C and D) with the equivalent sets in the proteins, and indicated that oxidation-sensitive cysteines were dispersed over a large number of proteins rather than aggregated onto a few. Overall, most peptides contained only one site of oxidation (88%); likewise, 60% of identified proteins had just one unique site.

Finally, we compared our redoxome with sets from related studies (Fig. 2B). A comparison with the H_2O_2 Cys-sensitive redoxomes generated found that 40% of the datasets from Akter et al. (2015a) and 35% of the datasets from Wang et al. (2012b) were identified in the Col-0 and *top1top2* redoxomes. Our data sets also included proteins, albeit at lower percentages, from the Arabidopsis stress-induced S-Glutathionylated dataset (Dixon et al., 2005), thiol-disulfide proteome of the chloroplast revealed by differential electrophoresis (Ströher and Dietz, 2008), OxiTRAQ redox-sensitive proteome (Liu et al., 2014), seed oxidized proteome (Job et al., 2005), sulfenome (Waszczak et al., 2014), and the S-nitrosylated proteome (Lindermayr et al., 2005). The somewhat limited overlap with published data may reflect differences in detection methodology, but also the type of stress applied—with the published data sets obtained following exogenous application of hydrogen peroxide. In total, considering all pathogen-treated and control samples, this study contributes 830 new putative redox-sensitive proteins associated with the ETI, and 548 redox-sensitive proteins not associated with the ETI.

Characterization and Comparative Analyses of the Col-0 and top1top2 Redoxomes

To uncover specific effects of TOP1 and TOP2 on redox-mediated processes during the ETI, we performed a comparative functional analysis of the Col-0 and *top1top2* redoxomes (Supplemental Table S2). A GO analysis showed strong enrichment for metabolic processes in both Col-0 and *top1top2*. GO biological processes (GOBPs) such as "oxidation-reduction process," "generation of precursor metabolites and energy," and "translation" were enriched in both genotypes (Fig. 3A). Chloroplast-specific GOBPs including pigment metabolism, heme biosynthesis, and thylakoid membrane organization were enriched only in Col-0; however, GOBPs related to the organization and synthesis of precursors for the cell wall (CW), endoplasmic reticulum protein degradation, and pathogen-induced cell death were uniquely enriched in *top1top2* (Fig. 3A). An analysis of the protein groups (GO Molecular Function) revealed commonalities but also marked dissimilarities among datasets (Fig. 3B). As such, in both redoxomes "oxidation-reduction activities" and proteins with "FeS cluster binding" properties, known for their role in the oxidation-reduction reactions of chloroplastic and mitochondrial electron transport (Dai et al., 2000), were significantly over-represented. However, whereas Col-0 was enriched in glutathione-disulfide reductases and phosphotransferases, the *top1-top2* redoxome had a high abundance of chitinases, peptidases, hexokinases, and thioredoxin-disulfide reductases. The quantitative and qualitative differences between Col-0 and *top1top2* redoxomes were further revealed by a pathway-enrichment analysis (Fig. 3C). Whereas both genotypes showed an over-representation of the pathways for proteasome degradation, glycolysis, and amino acid biosynthesis, they differed in the over-representation of distinct amino acid biosynthesis pathways.

We queried the UniProt database to retrieve protein functional and structural information. We found that greater than one-quarter of Col-0 and *top1top2* datasets (26% and 29%, respectively) contains proteins with annotated redox-associated PTMs (oxPTMs; Supplemental Fig. S3A**)**. Among the proteins with annotated PTMs, 38% in Col-0 and 53% in *top1top2* contained annotated redox-active Cys or structural disulfide bridges, thiol glutathionylation, and nitrosylation. Other types of PTMs with high representation in our datasets included N-acetylation and Ser/Thr phosphorylation. We asked next whether the position of sensitive cysteines within proteins corresponds to the annotated sites of Cys oxPTM (Fig. 3D). For the Col-0 dataset, annotations were available for 54 Cys sites in 18 proteins. We found that 15 annotated sites (in 13 proteins) were identified as oxidation-sensitive in Col-0 and an additional 11 sites (in eight proteins) were new sensitive sites identified. Altogether, almost 50% of the annotated redox-sensitive cysteines were discovered in the Col-0 dataset. For *top1top2*, annotations were available for 94 sensitive sites in 15 proteins. Specifically, we identified 17 annotated sites (located in 12 proteins), and seven additional sites (located in six proteins) without a UniProt annotation. Direct comparison of Col-0 and *top1top2* coverage is difficult due to the relatively low overlap between the two datasets; nevertheless, it appears that fewer annotated sensitive sites are oxidized in *top1top2* relative to Col-0.

Because many of the annotated redox-sensitive PTMs present in the redoxomes belong to well-known redox sensors or redox-modulated proteins, we took a closer look into the apparent disparity in the number of oxidized sites in Col-0 versus *top1top2* (Table 1). In the 20 proteins surveyed, 37 and, respectively, 29 cysteines were identified as oxidized in Col-0 and *top1top2*, indicating a 22% decrease in the number of oxidized sites in the mutant. The most affected proteins in *top1top2* were: the SA-binding BCA1 with functions in the ETI, chloroplastic magnesium-chelatase subunit ChlI-2, glutaredoxin C1, NADPH-dependent thioredoxin reductase3 for chloroplast protection against oxidative damage (Marty et al., 2009), chloroplastic thioredoxin M1 with roles in the oxidative stress, disulfide-isomerase PDI5-1, and chloroplastic dihydrolipoyl dehydrogenase2. Notably, the chloroplastic redox sensor 3'(2'),5'-bisphosphate nucleotidase 1 was identified as well; Cys-167 from the disulfide bridge 167-190, described as inhibitory under oxidizing conditions

(Chan et al., 2016), was oxidized in Col-0 but not in *top1top2*.

We considered whether the differences in oxidation patterns extend to the proteins categorized in GO as associated with defense or redox homeostasis in our datasets. An analysis of identifiers associated with "immune response," "SA signaling," and "programmed cell death" (Fig. 3E) and "cellular redox homeostasis" and "oxidative stress response" (Fig. 3F), identified overlapping and genotype-specific proteins. Common oxidized proteins include components of the Resistance-gene signaling (Century et al., 1995), SA signaling (MPK4, ROC1, and pathogenesis-related proteins [PR]1, PR2, and PR4; Sharma et al., 1996; Brodersen et al., 2006), and the SA-regulated catalase-1 and catalase-2 (Durner and Klessig, 1996). Known defense or oxidative stress markers, including the NPR1-dependent OPR1 (Blanco et al., 2005), PR4, and the cell death antagonist KTI1 (Li et al., 2008), had significantly different oxidation levels in the *top1top2* redoxome. To test the possibility that proteins in Figure 3, D and E, are connected functionally, information on their known and curated protein–protein interactions (PPI) was extracted from public repositories (Szklarczyk et al., 2016); the PPI network generated (Supplemental Fig. S3B; Supplemental Table S3**)** had significant PPI enrichment *P* values, indicating that most of these proteins are biologically connected. We used the software PathLinker (Huang et al., 2018) to assemble the PPIs in a putative signaling network (Supplemental Fig. S3C**)**,

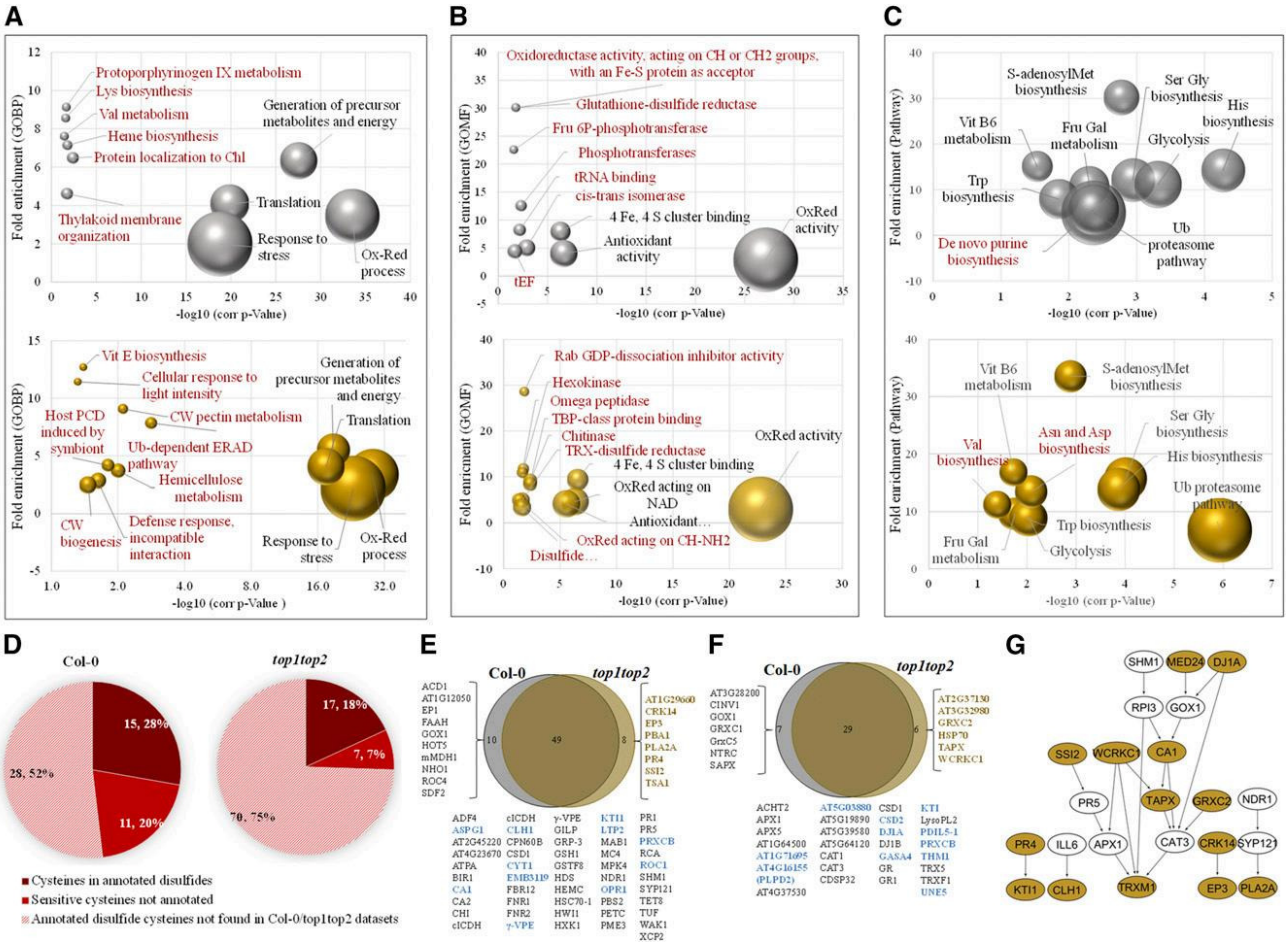

Figure 3. Comparison between Col-0 and *top1top2* reversible Cys redoxomes during the effector-triggered immune response. A to C, Enrichment of GOBP terms. GOBPs (A), GO molecular functions (GOMF; B), and Pathways (C) in Col-0 (gray) and *top1top2* (brown). Text in black shows GO terms/pathways common for Col-0 and *top1top2*, whereas text in red shows terms unique for each genotype. D, The frequency of annotated proteins with PTMs in Col-0 and *top1top2* redoxomes. E and F, Overlap and specificity in the Col-0 and *top1top2* redoxomes. Numbers represent the numbers of proteins in each category; colored text indicates proteins unique to *top1top2* (brown) or with differential oxidation in *top1top2* (blue). E, Common and unique proteins associated with the GO terms "defense to bacteria," "incompatible interaction," "hypersensitive response/PCD," "SA signaling," and "systemic acquired resistance." F, Common and unique proteins associated with the GO terms "oxidative stress response" and "cellular redox homeostasis." G, Predicted cellular pathways with defective protein Cys oxidation in *top1top2* plants. Nodes in brown are oxidized proteins unique for, or with, differential oxidation in *top1top2*. OxRed, oxidoreductase activity; Fru 6P, Fru 6-P tEF, translation elongation factor activity; Chl, chloroplast.

Table 1. *Proteins with annotated oxidation-sensitive cysteinesInformation about the position of disulfide bridges and Cys PTM were retrieved from UniProt and relevant literature (cited in the main text).*

Symbol	Protein Name	Disulfide Bond/PTM	Cys Oxidized in top1top2	Cys Oxidized in Col-0	Effects of Oxidation
BCA1/ SABP3	Beta carbonic anhydrase1, chloroplastic (Salicylic Acid Binding Protein3)	Cys-280 S-nitrosylated	230-257-277-280	167-173-230-277-280	S-nitrosylation at Cys-280 is up-regulated during nitrosative burst and blocks binding of SA and BCA1 activity
AMY3	Alpha-amylase3, chloroplastic	DISULFID 499-587	None	363	Redox-regulated, with the highest activity under reducing conditions. The disulfide between 499 and 587 inhibits catalysis
CDSP32	Thioredoxin-like protein, chloroplastic	DISULFID 219-222	219-222	219-222-253	Redox-active
CHLI2	Magnesium-chelatase subunit ChlI-2, chloroplastic	DISULFID 96-187 DISULFID 348-390	390	390	Redox regulation; active in reducing conditions, inactive in oxidizing conditions. TRX F and M mediate the reversible reductive activation of oxidized CHLI2
CP121	Calvin cycle protein CP12-1, chloroplastic	DISULFID 68-77 DISULFID 110-119	110	110	Only the oxidized protein is active in complex formation. The C-terminal disulfide is involved in the interaction with GAPDH. The N-terminal disulfide mediates the binding of PRK with this binary complex
CP122	Calvin cycle protein CP12-2, chloroplastic	DISULFID 75-84 DISULFID 117-126	117	126	
CYP20-3/ ROC4	Peptidyl-prolyl cis-trans isomerase, chloroplastic	DISULFID 131-248	None	206	PPIase activity is optimal in reduced form and minimal in oxidized form. Reduction of the oxidized form is mediated by TRX M
DSP4/ AtSEX4	Phosphoglucan phosphatase DSP4, chloroplastic (Dual Specificity Protein Phosphatase4; Protein StarchExcess4)	ACT_SITE 198	198-374	198-374	198 Phospho-Cys intermediate in the enzyme active site
FTRC	Ferredoxinthioredoxin reductase catalytic chain, chloroplastic	DISULFID 87-117	104-106-115-117	104-106-115-117	Redox-active
GRXC1	Glutaredoxin-C1 (AtGrxC1)	DISULFID 39-42	None	39-42	Redox-active
IF4E4/ LSP1	Eukaryotic translation initiation factor isoform 4E (Loss Of Susceptibility To Potyvirus1)	DISULFID 97-138	97	97	According to the redox status, the 97-138 disulfide bridge may have a role in regulating protein function by affecting its ability to bind capped mRNA
MSRB8	Peptide Met sulfoxide reductase B8	DISULFID 75-128	128	128	Redox-active
PDI51	Protein disulfideisomerase5-1	DISULFID 55-58	51-55-85	51-55-85	Redox-active
PGR5	Protein PROTON GRADIENT REGULATION5, chloroplastic	DISULFID 11-105	105	105	DISULFID11-105 bridge is probably involved in disulfide bridges with PGRL1A
PLPD2	Dihydrolipoyl dehydrogenase2, chloroplastic	DISULFID 122-127	122-127	122-127-397	Redox-active
SAL1	SAL1 phosphatase, chloroplastic	DISULFID 167-190	167	None	Oxidative stress sensor; disulfide bridge 167–190 inhibitory under oxidizing conditions
STR9	Rhodanese-like domain-containing protein9, chloroplastic; Sulfurtransferase9	ACT_SITE 145	145	145	Cys-145 in the active site is a persulfide intermediate
TRXB3	NADPH-dependent thioredoxin reductase3	DISULFID 217-220 DISULFID 454-457	None	454-457	Both disulfide bridges are redoxactive

(*Table continues on following page.*)

Table 1. (*Continued from previous page.*)

Symbol	Protein Name	Disulfide Bond/PTM	Cys Oxidized in top1top2	Cys Oxidized in Col-0	Effects of Oxidation
TRXF1	Thioredoxin F1, chloroplastic (Thioredoxin F2)	DISULFID 99-102 Cys-126 S-glutathionyl Cys transient	99-102	99-102	DISULFID99-102 Redox-active; Glutathionylation at Cys-126 decreases its ability to be reduced by FTRC and reduces its efficiency in activating target chloroplastic enzymes
TRXM1	Thioredoxin M1, chloroplastic	DISULFID 104-107	104-107	104-107	Redox-active

from which a subnetwork was retrieved including only the components with altered levels of oxidation in *top1top2* (Fig. 3G). In Figure 3G, 36% of the nodes are chloroplastic and mitochondrial oxidoreductases—including the thioredoxin ACHT2, peroxidases (SAPX, TAPX, and WCRKC1), the redox-regulated and redox shuttling malate dehydrogenase mMDH1 (Yoshida and Hisabori, 2016), the NADPH-dependent thioredoxin reductase C for protection against oxidative damage (Puerto-Galán et al., 2015), the superoxide dismutase CSD2, and the GOX1 oxidase that mediates ROS signal transduction in plant resistance (Rojas et al., 2012).

Overall, we identified known redox-regulated proteins in Col-0 and *top1top2* redoxomes, suggesting that they are active during the ETI; comparative analyses revealed the identity of the proteins and potential pathways with altered oxidation in *top1top2*, implicating oxidoreductases and defense components as a possible major disparity between genotypes.

Progressive Differences in Thiol Oxidation between Genotypes

We investigated the time dynamics of the Col-0 and *top1top2* redoxomes. When comparing oxidation levels at 8 hpi between the control and infection conditions, we identified 550 cysteines that mapped to 458 proteins in Col-0, and 444 cysteines that mapped to 375 proteins in *top1top2* (Supplemental Fig. S4A). In Col-0, 521 (95%) peptides increased, whereas 29 (5%) decreased in oxidation at 8 hpi relative to the 8 h control; by comparison, in *top1top2*, 393 (89%) increased, and 51 (11%) decreased in their relative oxidation levels. When comparing 8 hpi with 12 hpi, we found 596 peptides (485 proteins) in Col-0 and 555 significant peptides (465 protein identifiers) in the *top1top2* mutant with significantly changed oxidation state. In Col-0, 178 (30%) increased and 418 (70%) decreased at 12 hpi, whereas in *top1top2*, 212 (38%) increased and 343 (62%) decreased at 12 hpi, showing an overall decreased oxidation trend in both Col-0 and *top1top2*. This was the condition where Col-0 and *top1top2* exhibited the greatest difference regarding their Cys oxidation dynamics. In the control samples at 8 h, we identified 109 significant reversible oxidation changes between the genotypes; 66 (61%) were increasing in Col-0, and 43 (39.4%) were increasing in *top1top2*. A similar analysis was performed with the peptides showing time- or genotype-specific significant differences. Between Col-0 with *top1top2* at 8 hpi, 85 peptides were significantly different; 50 (58.8%) showed an increase in Col-0 whereas 35 (41.2%) were higher in *top1top2*. Finally, at 12 h, out of the 144 significantly modified cysteines identified, 70 (48.6%) increased in Col-0 and 74 (51.4%) in *top1top2*. We summarized the above-described changes in oxidation and plotted the net change at all time points (Fig. 4A). Overall, the redoxomes of Col-0 and *top1top2* showed a similar time-dependent dynamics—low oxidation at 8 h control, high increase in oxidation at 8 hpi, followed by a sharp decrease in the number of oxidized cysteines at 12 hpi. Notably, both the positive and negative fluctuations in net oxidation levels were larger in Col-0 than in *top1top2* at both 8 and 12 hpi.

To capture additional details on the temporal changes in oxidation and ascribe a functional identity to oxidized proteins, we utilized the time-series clustering package TMixClust (Golumbeanu and Beerenwinkel, (2018); R Development Core Team, 2018) to group peptides according to their oxidation dynamics patterns. We found 23 and 24 clusters, respectively, to be optimum settings for Col-0 and *top1top2* (Supplemental Fig. S4B). A cluster oxidation gradient measuring the average increase or decrease in the oxidation level of protein identifiers at 8 hpi and 12 hpi within each Col-0 or *top1top2* cluster was visualized using a heat map (Fig. 4B). A comparative inspection of the heat map revealed many clusters showing the wave pattern of oxidation described in Figure 4A—sharp increase in oxidation at 8 hpi followed by a decrease at 12 hpi. We quantified the range of increase/decrease in protein oxidation level and confirmed that it was higher in Col-0 (-8.4 to 4.8 Log_2 fold-change [LFC]; range: 13.2) than in *top1top2* (-6.0 to 3.9 LFC; range: 9.9). In Col-0, proteins associated with response to stress, including various peroxidases and proteins localized in chloroplast stromules and apoplast, had increased Cys oxidation at 8 hpi and decreased oxidation at 12 hpi (Fig. 4C).

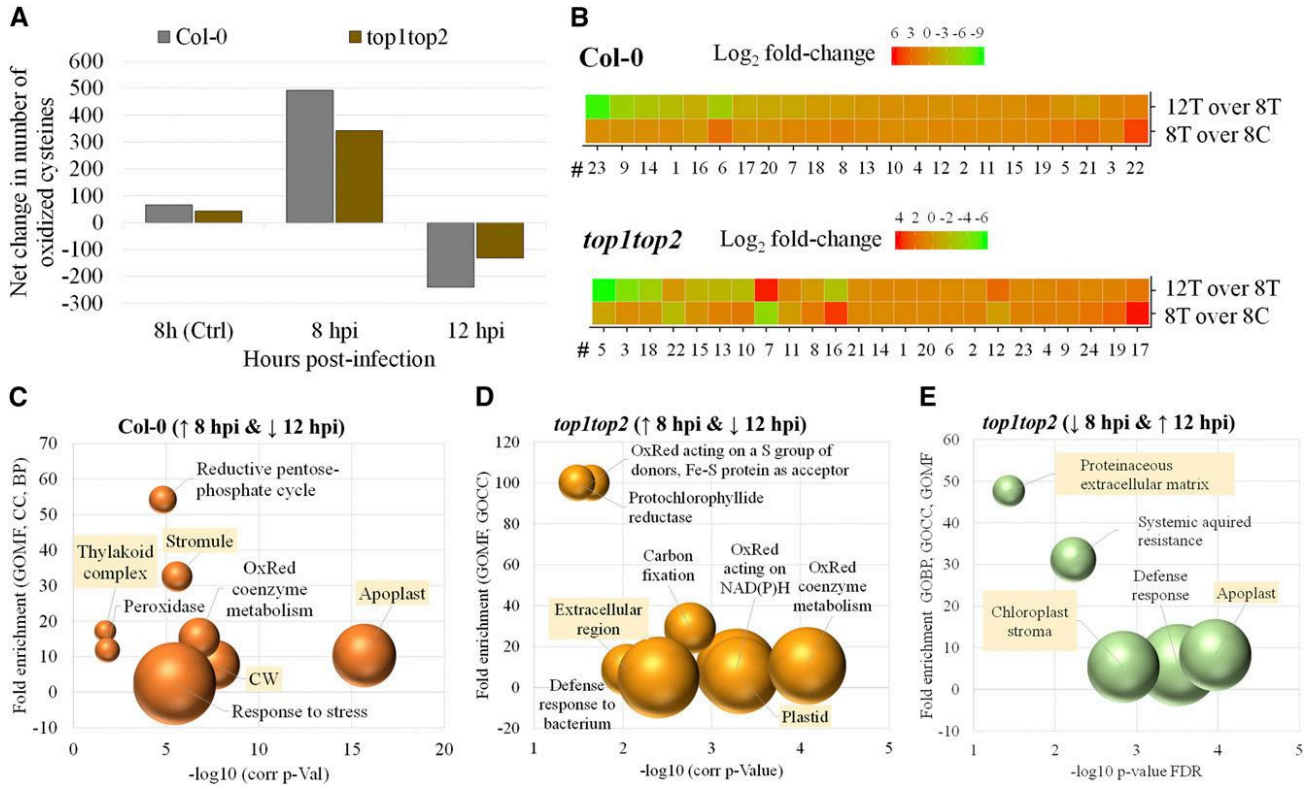

Figure 4. Reversible Cys oxidation during the plant immune response shows time-dependent dynamics. A, Net changes in protein Cys oxidation in Col-0 and *top1top2* plants during the ETI. Net oxidation was calculated by subtracting the number of peptides with reduced oxidation from the number of peptides with increased oxidization at each time point: Ctrl (8h-C), and 8 hpi and 12 hpi. B, Time-dependent oxidation dynamics in Col-0 and *top1top2* protein clusters. Average change was calculated between 8 hpi and 12 hpi, respectively, with *P. syringae* avrRpt2 and buffer control, respectively. Red/green colors indicate, respectively, a higher/lower LFC; orange shows neutral change (fold change of 1). C, GO enrichment in Col-0 clusters 1, 6, 9, 14, and 23 showing increased oxidation at 8 hpi and decreased oxidation at 12 hpi. D, GO enrichment in *top1top2* clusters 3, 5, 16, and 18 showing increased oxidation at 8 hpi and decreased oxidation at 12 hpi. E, GO enrichment in *top1top2* clusters 7, 12, and 22 showing decreased oxidation at 8 hpi and increased oxidation at 12 hpi. GOCC: GO cellular localization (shaded terms); OxRed: oxidoreductase activity.

Clusters with a similar wave dynamics in *top1top2* were enriched in oxidoreductases, porphyrin and chlorophyll metabolic enzymes, plastid-, and apoplast-localized proteins (Fig. 4D). Furthermore, cluster analysis identified *top1top2* proteins (69 identifiers grouped in clusters 7, 12, and 22) with significantly reduced oxidation at 8 hpi and increased oxidation at 12 hpi; this group was enriched in proteins associated with defense against bacteria and systemic acquired resistance localized in the apoplast, extracellular matrix, and chloroplast stroma (Fig. 4E).

Our results demonstrate that protein oxidation during ETI follows distinct time-dependent patterns; cysteines with similar dynamic profiles belong to proteins having common localizations, molecular functions, and participating in similar biological processes. Although Col-0 and *top1top2* manifested similar dynamics in protein oxidation, the amplitude of the oxidation wave was lower in *top1top2* than in Col-0; both fewer oxidized proteins and fewer oxidized cysteines per protein were identified in the mutant.

Structural Determinants of Cys Oxidation

Biochemical studies with metazoan proteins have identified several factors that determine the susceptibility of protein thiols (-SH) to oxidation, including thiol's acid dissociation constant (pK_a) and position within the native protein structure. At physiological pH, thiols with $pK_a < 7$ exist as thiolates (S^-) that have increased reactivity toward electrophiles such as oxidants. Exposure of thiolates on protein surface increases their proximity to the oxidant source and determines responsiveness to cellular redox environment. To identify possible specificity-determinants for Cys oxidation, we searched the Protein Data Bank with the complete list of oxidized proteins and retrieved complete 3D structures for 48 proteins (Supplemental Table S4) containing 518 cysteines of which, 104 (20%) were identified as oxidation-sensitive in the ETI redoxome.

To investigate the relationship between cysteines exposure on the protein surface, acidity, and their

susceptibility to oxidation, we calculated the surface accessibility ("buried" B coefficients) and pK_a values of their cysteines using the software PROPKA v2.1 (Rostkowski et al., 2011). Overall, 34% of cysteines were defined as "exposed" ($B \leq 60$) and 66% as "buried" ($B > 61$). Although similar percentages among the buried (25%) and exposed cysteines (21%) were found as oxidized, the cysteines with low solvent-exposure predominated in the oxidized cohort (Fig. 5A). An analysis of the distribution of the B values in oxidized versus nonoxidized residues showed that oxidized cysteines segregated into two distinct groups. Among the "buried" cysteines, the oxidized sites were significantly less solvent-exposed than the nonoxidized sites; on the other hand, among the solvent-exposed cysteines, the oxidized sites had significantly higher solvent-exposure than the nonoxidized sites (Fig. 5B). A similar analysis performed using the pK_a values of cysteines determined that surface-exposed sites had significantly lower predicted pK_a values (average pK_a = 9.7) than

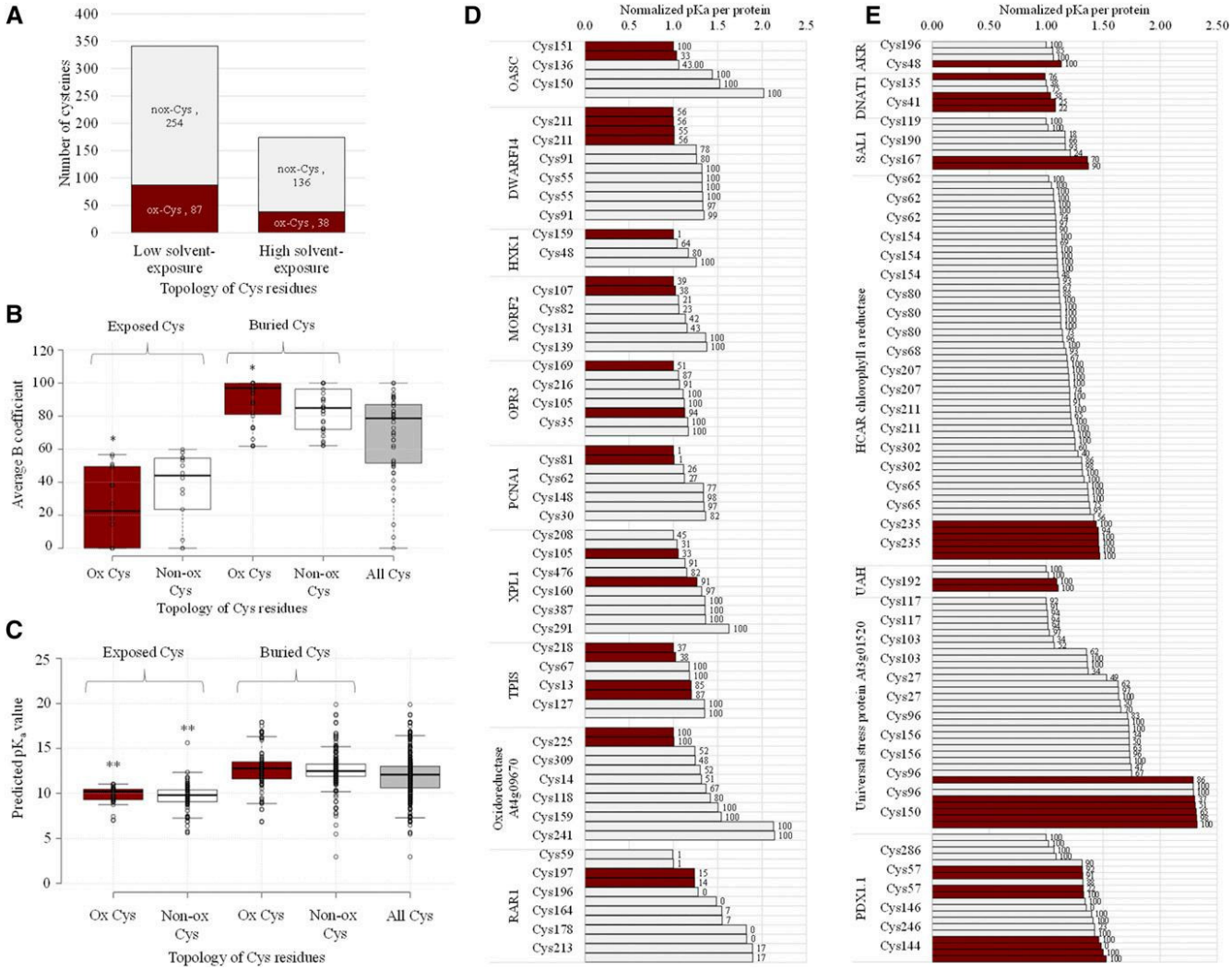

Figure 5. Structural determinants of Cys oxidation in the Arabidopsis proteome. A, Protein Cys residues having low or high solvent exposure in a subset of the Col-0 and *top1top2* redoxomes, found to be oxidized (ox-Cys) or unmodified (nox-Cys). B, Distribution of ox-Cys and nox-Cys according to their average of solvent exposure. "All Cys" shows the distribution of average B coefficients/protein for all cysteines analyzed. The asterisks show statistical relevance ($P < 0.05$, Student's t test parameters: two-tailed distribution, two-sample unequal variance) between the exposed and buried cysteines. C, The distribution of pK_a values for oxidized cysteines with high (Exposed Cys) and low solvent-exposure (Buried Cys). Statistically, significant differences ($P < 0.01$) are shown between exposed and buried cysteines for both oxidized and nonoxidized Cys groups. D, The distribution of pK_a values within proteins in which solvent-exposed cysteines ($B < 61$) were found to be sensitive to oxidation. E, The distribution of pK_a values within proteins in which cysteines with low solvent-exposure were identified as oxidation sensitive. In (D) and (E), values above bars are the B coefficients of cysteines. The analyses were performed on 514 Cys residues in 48 proteins. The asterisks show statistical relevance ($P < 0.05$, Student's t test parameters: two-tailed distribution, two-sample unequal variance). The position of each Cys residue is shown on the x axis, and the residues were arranged in the order of increasing pK_a value. (Red) Oxidized residues; (left) UniProt (or Araport) protein identifiers.

buried cysteines (average pK_a = 12.7); however, we found no relevant differences between the oxidized and nonoxidized cysteines (Fig. 5C). We considered the possibility that potential differences in the reactivity of the oxidized cysteines are hidden in this analysis due to the relatively large number of sites per protein and the large variation in their pK_a values. To account for these variations, the pK_a values for each protein were normalized. An inspection of the normalized pK_a values in proteins with "buried" or "exposed" oxidized cysteines, revealed patterns recurring in at least half of the proteins analyzed. Fig. 5D shows 10 proteins where the "exposed" oxidized cysteines have the lowest pK_a values within the respective proteins. This group includes Cys-65 in the sugar sensor hexokinase1 (HXK1; Jang et al., 1997), Cys-136 in the O-acetyl-Ser (thiol) lyase OASC, Cys-211 in the hydrolase DWARF14, Cys-169A in the oxidoreductase OPR3, aCys309 in the oxidoreductase At4g09670, and Cys-197 in the Cys- and His-rich domain of RAR1 (Kadota et al., 2008). On the other hand, we found 11 proteins (seven of them shown in Fig. 5E) where the "buried" oxidized cysteines have the highest pK_a values within each protein. This set included Cys-48 in the chloroplastic NADPH-dependent aldo-keto reductase, Cys-40 and Cys-41 in the phylloquinone biosynthesis hydrolase DHNAT1, Cys-167 in SAL1, and Cys-235 in the chlorophyll catabolic enzyme HCAR. In these proteins, buried cysteines may be oxidized following interactions with ROS-sensors such as peroxidases.

Overall, our results demonstrate that both surface-exposed and internal cysteines are sensitive to oxidation; exposed cysteines with the lowest pK_a values or buried cysteines with the highest pK_a values within a protein are susceptible to oxidation, suggesting a remarkable specificity in protein thiol oxidation and a possible mechanism.

DISCUSSION

A Mass Spectrometry Label-Free Approach to Characterize Plant Redoxomes—Methodological Considerations

To study the dynamic reversible oxidation of protein cysteines in Arabidopsis, we used a tag-switch assay to enrich modified proteins, wherein in vivo reduced thiols were blocked by IAM before reduction of all reversibly oxidized sites and enrichment using TPS6B resin. This methodology has been used extensively in the study of reversible oxidation with considerable success in diverse biological systems (Forrester et al., 2009; Paulech et al., 2013; Guo et al., 2014a, 2014b). Although generally susceptible to false-positive identifications of reversibly oxidized sites due to incomplete alkylation of reduced cysteines, we performed a control experiment to ensure that the reaction was sufficiently complete (Supplemental Fig. S1A). Label-free approaches rely on the mass spectrometric signal intensity of peptide precursor ions across separate LC-MS/MS acquisitions for relative quantification. Whereas isobaric labeling techniques provide higher precision and faster acquisition when comparing multiple sample types, label-free workflows allow enhanced proteome coverage and improved linear range of quantitation at a greatly reduced cost to the researcher (Wang et al., 2012a; Dong et al., 2015). Therefore, we opted to use a workflow incorporating LFQ utilizing our protein-level TPS6B enrichment. Our robust LFQ measurements following this enrichment technique allowed differential analysis of the redoxome with increasing duration post-bacterial challenge in Col-0 and *top1top2*. We discovered that Cys reactivity in both redoxomes was strongly correlated with previously annotated sites of reactive Cys residues part of redox-active sites, disulfide bridges, or cysteines modified by reversible oxPTM including glutathionylation and nitrosylation. It is important to notice that our method may not have identified all sensitive cysteines because of their inaccessibility to label and low cellular abundance. These changes were used to elucidate both temporal and genotype-specific Cys oxidation to the biotic stress as a first principle, albeit we recognize that changes in protein abundance could falsely skew the measured fold changes attributed to Cys oxidation. We, therefore, take the findings of this study as a necessary guide for researchers to potentially responsive Cys-sites, with the caveat that the actual protein abundance may change.

Nevertheless, the results from the literature and database mining indicate that a large percentage of the reactive cysteines we identified are located in proteins with known oxPTM or redox-active sites. Even though additional validation of the oxidized cysteines discovered in this study is required, we have drastically increased the current repository of reversible oxPTMs on cysteines and substantiated previous studies of oxidation-sensitive proteins. We found that most proteins have one or few sensitive Cys sites and sensitive sites are present in a large number and diverse classes of proteins, suggesting the extensive oxidation of the ETI proteome.

How do TOP1 and TOP2 Contribute to the Redox Proteome Phenotype?

Data presented in this article brings information on the impact of TOP1/TOP2 on the composition of the Cys-oxidized proteome in the early stages of the ETI and highlights the contributions of TOP1/TOP2 to achieving and maintaining proper levels of oxidation during the oxidative burst. Plants contain numerous proteases, and many are known to participate in immune signaling and HR initiation or execution (van der Hoorn, 2008). Barring a few exceptions (Breitenbach et al., 2014; Zhang et al., 2014), the coordination of pathogen defense pathways with the action of proteases is insufficiently understood (van der Hoorn, 2008). Several mechanisms could contribute to the impaired

regulation of ETI redox homeostasis in *top1top2*. Akin to FtsH proteases (Yoshioka-Nishimura et al., 2014), TOP1 oligopeptidase activity may ensure the optimal productivity of the photosystem complexes as part of the chloroplast quality control machinery and may function in the light-dependent pathway that controls the magnitude of cell death (Kangasjärvi et al., 2014; Stael et al., 2015). On the other hand, TOP2 appears to operate in parallel, or the aftermath of, the chloroplastic oxidative burst. TOP2 may participate in the degradation of irreversibly oxidized proteins downstream of the 20S proteasome to decelerate cell death and spatially restrict the HR. A more precise function can be envisioned whereby TOP2 may generate signaling peptides to suppress cell death and activate immune responses through the H_2O_2-induced signaling that controls redox homeostasis (Nakagami et al., 2006) or ETI-associated pathways (Fu et al., 2012; Spoel and Dong, 2012) known to function in a proteasome-dependent manner.

Variation in net protein oxidation and number of oxidized cysteines observed between or within the genotypes could be a consequence of several mechanisms. The increase in the oxidation levels of a protein can result from an upsurge in its oxidation when the protein maintains its steady-state abundance, from an increase in its abundance with steady-state oxidation, or a combination of both. Conversely, the decrease may originate from either steady-state oxidation on a proteolytically degraded protein, reduction of cysteines on a protein in steady-state abundance, irreversible oxidation of cysteines on a protein in steady-state abundance, or combination of the three. Each possibility would increase/decrease relative abundance measured in our assays. Notably, loss of both *TOP1* and *TOP2* has no significant effects on plant development, growth, and reproduction under physiological conditions (Moreau et al., 2013). Thus, rather than having generalized proteolytic housekeeping functions, TOPs are likely to have specialized roles that manifest under plant stress, akin to the chloroplastic proteases from the Clp system found to have a small and specialized repertoire of substrates (Nishimura and van Wijk, 2015). A more precise answer regarding TOP1/TOP2 contributions to the redoxome phenotypes, additional knowledge is needed on their function to plant proteostasis and the identity of their substrates.

So far, based on our results, we anticipate that pathways and processes activated in the plant during the immune response, including signaling and metabolic pathways, are the probable subjects of regulation through oxPTMs. Significant changes occur in *top1top2* in the composition of the redoxome and the total number of Cys sites oxidized. To expand on this hypothesis, let us examine our findings from this perspective. The molecular players activated as part of the innate immune response are fairly well known. In resistant plants, the avrRpt2-mediated degradation acts as a signal for RPS2 activation. A critical component is the cyclophilin ROC1 (Aumüller et al., 2010) that activates *P. syringae*'s putative Cys-protease AvrRpt2 (Coaker et al., 2005). Whereas in Col-0, both Cys-69 and Cys-122 of ROC1 were oxidized, only Cys-122 was detected in the mutant; also, the related ROC4 was found oxidized exclusively in the Col-0. The oxidation-sensitivity of ROCs is consistent with reports ascribing oxPTMs and redox-regulation to cyclophilins (Shapiguzov et al., 2006; Campos et al., 2013). Protein-folding machinery is required for transduction of R-gene mediated resistance (Holt et al., 2005). Cys-43 in the CHORD domain of the cochaperone RAR1 was identified in both Col-0 and *top1top2*; however, the infection-triggered chaperone HSP70 was differentially oxidized. Furthermore, PLTP2, a PCD regulator from the PR14 family (Sels et al., 2008) has four disulfide bonds; the sensitive Cys-100 was oxidized in both Col-0 and *top1top2*. The SA-inducible PR1, PR4, and PR5 were also identified as sensitive to oxidation. The potential redox-regulation of PRs is supported by the finding that PR5 is a possible target of thioredoxins (Marchand et al., 2006) and that PR1 accumulation is under the regulation of glutathione (Senda and Ogawa, 2004). Peptidases implicated in immune-related processes at the CW and extracellular matrix were identified as possible redox-modulated proteins. The SA-inducible Gly-rich protein3 participates in CW repair; four residues (Cys-82/86/87/94) in Gly-rich protein3 Cys-rich motif required for the oxidative cross linking to CW (Domingo et al., 1999) were oxidized in both genotypes. ASPG1, an aspartyl protease induced locally and systemically during systemic acquired resistance (Breitenbach et al., 2014); out of the six structural disulfides, Cys-271 was found differentially oxidized in *top1top1*. Cys-292 in the PCD-regulator XCP2 peptidase (Zhang et al., 2014) was oxidized in both genotypes. Lastly, Cys peptidases from the metacaspase family were found to be oxidation-sensitive. In MC4, a positive PCD regulator (Watanabe and Lam, 2011), Cys-22 and the catalytic Cys-139 were oxidized in both genotypes; s-nitrosylation of Cys-139 regulated the activity of MC9 (Vercammen et al., 2004; Belenghi et al., 2007).

Primary metabolism, especially pathways necessary for producing energy and metabolites, are critical to the execution of plant defense responses. Transcriptional down-regulation of genes involved in photosynthesis and chlorophyll biosynthesis accompanies responses to avirulent pathogens (Apel and Hirt, 2004; Rojas et al., 2014). Considering the significant over-representation in our datasets of carbohydrate metabolism, photosynthesis, and photorespiration pathways, we postulate that changes in the redox homeostasis during the ETI are liable to be involved in the regulation of enzymatic activities acting in these pathways. The link between carbohydrate metabolism and defense responses is best exemplified by the activity of HXK1, a sugar-sensor that controls the transcriptional induction of PR1 and PR5 (Xiao et al., 2000). Cys-159, in the proximity of the HXK1 sugar-binding site, was found oxidized in both Col-0 and *top1top2*. In *top1top2*, BCA1/SABP3, required for photosynthesis and CO_2 signaling

and known to be inactivated by oxidation or S-nitrosylation of Cys-280 (Wang et al., 2009; Nienaber et al., 2015), was found underoxidized relative to Col-0. Several enzymes with roles in chloroplast biogenesis and photosynthetic pigment synthesis were differentially oxidized in *top1top2*. ACD1, an FeS cluster oxygenase that functions in chlorophyll catabolism and the ETI (Yao and Greenberg, 2006), was oxidized only in Col-0, whereas CHLI2, an Mg-chelatase that catalyzes chlorophyll biosynthesis and active only under reducing conditions (Kobayashi et al., 2008), was oxidized at higher levels in *top1top2*. Altogether, the altered patterns of oxidation in *top1top2* of components of resistance as well as metabolic pathways suggest the role of the TOP oligopeptidases in regulating their catalytic activity and, possibly, accumulation during the ETI.

Determinants of Cys Sensitivity and Specificity in Protein Oxidation

Systematic and thorough identification of cysteines undergoing oxPTMs under various conditions will help recognize possible general criteria in Cys sensitivity and specificity, and define redox switches and mechanisms of signal transmission. Our analysis focused on the chemical and structural properties of cysteines in a subset of proteins from the Arabidopsis reversible Cys redoxome. We aimed to use information on the solvent-exposure of thiols and their predicted pK_a values to identify commonalities among oxidized cysteines. In agreement with previous findings on thiol reactivity (Conte and Carroll, 2013), a set of the experimentally identified oxidized cysteines had high solvent-accessibility and the lowest predicted pK_a values within the respective proteins.

Interestingly, we also identified oxidized cysteines with low solvent-exposure and high pK_a values. Considering that thiols with higher pK_a values are strong nucleophiles and, thus, more reactive (Fernandes and Ramos, 2004), it is possible that they are targets of oxidation in vivo. Several caveats have to be mentioned here. First, because pK_a values of protein cysteines vary with the pH and subcellular localization, oxidation of proteins is modulated by its localization and the type of ROS that oxidize it (Foyer and Noctor, 2016). Second, the in vivo reactivity of protein thiols may differ from our predictions. Third, denaturing conditions in our protocol may have unavoidably exposed buried thiols that otherwise may not be susceptible to oxidation. Nevertheless, overall, our results strongly support a high specificity in plant thiol oxidation that cannot be solely the result of overall thiol reactivity. Potential mechanisms of protein oxidation may involve interactions between ROS sensors such as thiol peroxidases with protein substrates in thiol oxidizing relays (Sobotta et al., 2015), and self-sensitization mechanisms where the initial oxidation of an exposed thiol may cause local structural changes in the native protein structure to expose buried thiols.

MATERIALS AND METHODS

Plant Growth

Seeds of Arabidopsis (*Arabidopsis thaliana*; ecotype Columbia) and a double-knockout mutant of both *TOP1* (AT5G65620) and *TOP2* (AT5G10540) genes (Moreau et al., 2013) were sown individually in 24-hole plug trays containing soil. After stratification for 2 d at 4°C in the dark, plants were cultivated in a growth chamber for four weeks under medium-day conditions (12 h light/12 h dark) at 22°C and 60% relative humidity with 150 μmol/m^{2}s photon flux density.

Plant Infection

Pseudomonas syringae pv. *tomato* (*Pst*) avrRpt2 was freshly streaked from a glycerol stock onto King's B medium plates containing 100 mg/L rifampicin and 25 mg/L kanamycin and incubated at 28°C for 3 d. Bacterial cells were scraped from the plate, resuspended in 0.1 M sucrose in 10 mM $MgCl_2$ solution, and incubated at 28°C until OD_{600} of 0.1 was achieved. Three- to four-week-old plants were syringe-infiltrated to saturation with 1×10^5 CFU/mL *Pst* DC3000 *avrRpt2* suspended in 10 mM $MgCl_2$. Six leaves from each plant were syringe-infiltrated with either 10 mM $MgCl_2$ (mock) or bacteria (treatment), and plants were then moved back to the growth chamber. Plants mock-inoculated with 10 mM $MgCl_2$ solution were harvested after 8 h to serve as experimental controls. Otherwise, after 8 hpi or 12 hpi, leaves were excised from plants by cutting the petiole with a razor blade and immediately frozen under liquid nitrogen before storage at −80°C.

Ion Leakage Measurements

Three- to four-week-old plants were syringe-infiltrated, five leaves per plant, to saturation with 1×10^6 CFU/mL *Pst* DC3000 *avrRpt2* to elicit the oxidative burst and HR. Conductivity was used as a quantitative measure of ion leakage due to PCD. For each replicate, five leaf discs (1 per each of the five inoculated leaves) were collected from noninfiltrated leaf halves at 0, 4, 8, and 12 hpi and floated abaxial side up on MQH_2O. Leaf discs were shaken at 60 rpm at room temperature for 2 h before measuring the conductivity of the bathing solutions. Plants infiltrated with 10 mM $MgCl_2$ served as controls for ion leakage caused by $MgCl_2$ and wounding during infiltration. Total ion content was measured for each replicate after freezing and thawing the leaves within their respective bathing solutions. Four replicates were analyzed for each infiltration group per time point per line. Significant differences in comparison to Col-0 plants after *Pst*-infiltration were calculated using Student's *t* test parameters: two-tailed distribution, two-sample unequal variance.

Protein Extraction

Three biological replicates were used for 8-h mock-inoculated control, 8-hpi, and 12-hpi conditions for each genotype (e.g. Col-0 and *top1top2* mutants). Proteins were extracted using a Tris-buffered phenol method described in Slade et al. (2015). Briefly, leaf tissue (0.2 g) was ground under liquid N to a fine powder before homogenization in 2 mL of buffer containing 50 mM Tris (pH 8), 1 mM EDTA, 0.9 M sucrose, protease inhibitors (EDTA-free; Roche), and 100 mM IAM before adding SDS to a 1% (v/v) final concentration. The homogenate was incubated at room temperature for 90 min on a Techne rotator at 10 rpm to effectively block all in vivo reduced thiols. Proteins were then extracted from the aqueous phase by adding an equal volume (2 mL) of Tris-buffered phenol, pH 8 and mixing for 1 min before centrifugation (20,000*g*, 5 min). The top layer of phenol was separated to a prechilled tube, and an equal volume of Tris-buffered phenol was added to back-extract the aqueous phase. Proteins were precipitated from the combined phenolic layers using five volumes of cold 100 mM ammonium acetate in methanol and incubated at −80°C for 1 h before centrifugation (2,000*g*, 5 min). The resulting pellet was washed twice with 100 mM ammonium acetate in methanol and once with 70% (v/v) ethanol. The precipitate was resuspended in 50 mM Tris (pH 8.0), 0.5% (v/v) SDS, and 8 M urea and remaining cellular debris was removed by centrifugation (2,000*g*, 5 min). Protein concentration in the supernatant was determined using the 2D-Quant Kit (GE Healthcare) against BSA standard. Reversibly oxidized thiols were reduced using 10 mM DTT and incubated in a Thermomixer for 1 h at 37°C and 850 rpm. Excess DTT was removed by loading protein sample to an Amicon Ultra-0.5 centrifugal filter (EMD Millipore) with 10 kD MWCO and centrifuging for 10 min at 4°C and 10,000*g*. Washing buffer was then added

containing 50 mM Tris, pH 8 with 1 mM EDTA and 0.5% SDS in two passes. Protein was recovered from the filter using an equal volume of washing buffer and estimated for concentration. Subsequent enrichment of nascent thiols was performed using 500 μg of protein.

Protein-Level Cys Enrichment

Detailed evaluation of the steps used in the enrichment of reversible Cys oxidation was performed as described in Berg et al. (2019). Briefly, each replicate and 50 mg of TPS6B (GE Healthcare Bio-Sciences) resin slurry were combined and incubated in a Thermomixer for 2 h at 30°C and 850 rpm to allow protein binding via Cys thiols. Nonspecifically bound proteins were removed by washing the resin twice with 10 bed volumes each of washing buffer, washing buffer with 2 M NaCl, 70% (v/v) acetonitrile with 0.1% (v/v) trifluoroacetic acid (TFA), and finally 50 mM Tris, pH 8. On-resin digestion of Cys-bound proteins was performed by resuspending protein-resin slurry in 500 μL of 50 mM Tris, pH 8 before adding 10 μg of Trypsin Gold (Promega). The mixture was incubated in a Thermomixer for 3 h at 37°C and 850 rpm before separating peptide flow-through from bound Cys-proteins via brief centrifugation. Samples were then washed with 10 bed volumes each of washing buffer with 2 M NaCl, 70% (v/v) acetonitrile with 0.1% (v/v) TFA, and 50 mM Tris, pH 8. Bound Cys-containing peptides were eluted from the resin twice using 250 μL of 10 mM Tris, pH 8 with 50 mM DTT for 15 min.

LC-MS/MS Analysis

Samples were desalted using 50 mg Sep-Pak C18 cartridges before resuspension in 3% (v/v) acetonitrile with 0.1% (v/v) TFA and 5 mM DTT to prevent oxidation of reduced thiols before LC-MS/MS analysis. Peptides were analyzed using a NanoAcquity UPLC system (Waters) coupled to a TripleTOF 5600 mass spectrometer (AB Sciex). Mobile phase A consisted of water with 0.1% (v/v) formic acid and mobile phase B was acetonitrile with 0.1% formic acid. Peptide mixtures were injected to a Symmetry C_{18} trap column (100 Å, 5 μm, 180 μm × 20 mm; Waters) with a flow rate of 5 μL/min for 3 min using 99.9% A and 0.1% B. Peptides were then separated on an HSS T3 C_{18} column (100 Å, 1.8 μm, 75 μm × 250 mm; Waters) using a linear gradient of increasing mobile phase B at a flow rate of 300 nL/min. Mobile phase B increased to 35% in 90 min before ramping to 85% in 5 min, where it was held for 5 min before returning to 5% in 2 min and re-equilibrating for 13 min. The mass spectrometer was operated in the positive polarity and high sensitivity mode. MS survey scans were accumulated across an m/z range of 350–1600 in 250 ms. For information-dependent acquisition, the mass spectrometer was set to automatically switch between MS and MS/MS experiments for the first 20 features above 150 counts having +2 to +5 charge state. Precursor ions were fragmented using rolling collision energy ±5% with an accumulation time of 85 ms. Dynamic exclusion for precursor m/z was set to an 8-s window. Automatic calibration was performed every 8 h using a tryptic digest of BSA protein standard to maintain high mass accuracy in both MS and MS/MS acquisition.

Database Searching and Label-Free Quantification

Acquired spectral files (*.wiff) were imported into Progenesis QI for Proteomics (Nonlinear Dynamics, version 2.0). A reference spectrum was automatically assigned, and total ion chromatograms were then aligned to minimize run-to-run differences in peak retention time. Each sample received a unique factor to normalize all peak abundance values resulting from experimental variation. Alignment was validated (>80% score) and a combined peak list (*.mgf) for all runs was exported for peptide sequence determination and protein inference by the software Mascot (Matrix Science, version 2.5.1). Database searching was performed against the UniProt reference proteome (39,196 canonical entries) for Arabidopsis (www.uniprot.org/proteomes/UP000006548; accessed September 2017). Sequences for common laboratory contaminants (www.thegpm.org/cRAP; 116 entries) were appended to the database. Target-decoy searches of MS/MS data used a trypsin protease specificity with the possibility of two missed cleavages, peptide/fragment mass tolerances of 15 ppm/0.1 Da, and variable modifications of acetylation at the protein N terminus, carbamidomethylation at Cys, deamidation at Asn or Gln, and oxidation at Met. Significant peptide identifications above the identity or homology threshold were adjusted to <1% peptide FDR using the embedded Percolator algorithm (Käll et al., 2007) and uploaded to Progenesis for peak matching. Identifications with a score <13 were removed from consideration in Progenesis before exporting "Peptide Measurements" from the "Review Proteins" stage.

Data Availability

The mass spectrometry proteomics data have been deposited to the ProteomeXchange Consortium (www.proteomexchange.org) via the PRIDE partner repository (Vizcaíno et al., 2014) with the dataset identifiers PXD010104 (Username: reviewer56000@ebi.ac.uk, Password: 9HwxLtFp).

Data Preprocessing

Data were parsed using custom scripts written in the Python programming language. In the "Peptide Measurements" export, there were instances of rows with duplicated peak features and differing peptide identifications. Some features were matched with peptides having identical sequence, modifications, and score, but alternate protein accessions. These groups were reduced to satisfy the principle of parsimony and represented by the protein accession with the highest number of unique peptides, else the protein with the largest confidence score assigned by Progenesis. Some features were also duplicated with differing peptide identifications and were reduced to a single peptide with the highest Mascot ion score. Results were limited to only peptides with one or more Cys-sites of reversible oxidation, defined here as the absence of carbamidomethylation on at least one Cys residue in the peptide sequence. An identifier was then made by joining the protein accession of each feature with the particular site of Cys-oxidation in the protein sequence. Each dataset was then reduced to unique identifiers by summing the abundance of all contributing features (i.e. peptide charge states, missed cleavages, combinations of additional variable modifications). Each identifier group was represented by the peptide with the highest Mascot score in the final dataset.

Data Analysis

Linear Models Analysis and Missing Data Imputation

We employed the data analysis pipeline described in detail in Berg et al. (2019). The first step is the filtering of data features where all samples were outliers (Tukey's lower fence with $k = 1.5$). We then stabilized the variance of datasets by performing a $\log_2$-tranformation of all abundance values. We then perform missing data imputation method using random sampling from a normal distribution with parameters robustly estimated from the entire dataset (mean value for the imputation is calculated per Cys for all nonmissing values in each condition, or using Tukey's lower fence with $k = 2$ if all values are missing in one condition; SD for the imputation is computed per condition by taking the median of SDs of each Cys with nonmissing values; Berg et al., 2019). We quantify relative changes in peptide abundance between conditions using the *limma* R package (Ritchie et al., 2015). We applied a LFC change cut-off of ±1, and a false-discovery-rate–corrected P value cut-off of 0.05 to identify significantly altered oxidation of cysteines. Multiple imputations were used in conjunction with a binomial test to decide on statistically significant changes in proteome quantitation due to missing data. Each dataset was run through *limma* using lmFit with the *method = "robust"* flag and then eBayes using the default settings (Phipson et al., 2016). LFC was then calculated for each feature, comparison, and dataset. We modeled the outcome of the data imputation using a binomial distribution and performed a right-tailed binomial test (R's core feature binom.test; R Development Core Team, 2018) to identify the peptides with an outcome > 0.5, at a significance level 0.05.

Time-Series Clustering

We used the TMixClust time-series clustering R package. We chose a cluster size corresponding to the highest likelihood indicated by the stability analysis; we used the silhouette technique to validate cluster consistency. Each cluster size was run 20 times (nb_clustering_runs), and the number of clusters was iteratively incremented starting at two. Each run had a limit of 20 Monte Carlo resamplings using mc_em_iter_max, and 2,000 iterations of the expectation-maximization algorithm, to increase the precision of each run.

Functional Annotation

We used Araport (https://apps.araport.org/thalemine) annotations, Panther GO (http://pantherdb.org/) tools, and a statistical overrepresentation test (Fisher's Exact with false-discovery-rate multiple test correction) to perform functional analysis of significantly differentially oxidized Cys residues.

Structure-Reactivity Analysis

We used the software PROPKA 2.1 (http://nbcr-222.ucsd.edu/pdb2pqr_2.0.0/) to predict pKa and B values of cysteines in selected proteins with 3D structure information from the Protein Data Bank (https://www.rcsb.org/).

Set Analysis

To compare our redoxomes with public datasets we used the R package UpSetR to visualize the intersecting sets and their properties (Conway et al., 2017). We also used UpSetR to plot the unique common sets of proteins or Cys identifiers from selected combinations of pairwise comparisons.

Accession Numbers

Sequence data from this article can be found in the GenBank/EMBL data libraries under accession numbers listed in Supplemental Table 1.

Supplemental Data

The following supplemental materials are available.

Supplemental Figure S1. Supplementary material for Figure 1.

Supplemental Figure S2. Supplementary material for Figure 2.

Supplemental Figure S3. Supplementary material for Figure 3.

Supplemental Figure S4. Supplementary material for Figure 4.

Supplemental Table S1. Results of the label-free quantification of redox Cys-site identifiers and comparisons among genotypes and treatments.

Supplemental Table S2. GO overrepresentation tests in Col-0 and *top1top2* redoxomes.

Supplemental Table S3. The PPI network of proteins classified in GO terms related to plant defense and oxidative stress response.

Supplemental Table S4. PROPKA analysis of proteins with known 3D structures from Col-0 and *top1top2* redoxomes.

Received October 31, 2018; accepted November 16, 2018; published December 3, 2018.

LITERATURE CITED

Akter S, Huang J, Bodra N, De Smet B, Wahni K, Rombaut D, Pauwels J, Gevaert K, Carroll K, van Breusegem F (2015a) DYn-2 based identification of Arabidopsis sulfenomes. Mol Cell Proteom **14:** 1183–1200

Akter S, Huang J, Waszczak C, Jacques S, Gevaert K, van Breusegem F, Messens J (2015b) Cysteines under ROS attack in plants: A proteomics view. J Exp Bot **66:** 2935–2944

Alvarez S, Galant A, Jez JM, Hicks LM (2011) Redox-regulatory mechanisms induced by oxidative stress in *Brassica juncea* roots monitored by 2-DE proteomics. Proteomics **11:** 1346–1350

Apel K, Hirt H (2004) Reactive oxygen species: Metabolism, oxidative stress, and signal transduction. Annu Rev Plant Biol **55:** 373–399

Aumüller T, Jahreis G, Fischer G, Schiene-Fischer C (2010) Role of prolyl *cis/trans* isomers in cyclophilin-assisted *Pseudomonas syringae* AvrRpt2 protease activation. Biochemistry **49:** 1042–1052

Belenghi B, Romero-Puertas MC, Vercammen D, Brackenier A, Inzé D, Delledonne M, van Breusegem F (2007) Metacaspase activity of *Arabidopsis thaliana* is regulated by s-nitrosylation of a critical cysteine residue. J Biol Chem **282:** 1352–1358

Berg P, McConnell EW, Hicks LM, Popescu SC, Popescu GV (2019) Evaluation of linear models and missing value imputation for the analysis of peptide-centric proteomics. BMC Bioinformatics **20 (Suppl 2):** 102

Blanco F, Garretón V, Frey N, Dominguez C, Pérez-Acle T, van der Straeten D, Jordana X, Holuigue L (2005) Identification of NPR1-dependent and independent genes early induced by salicylic acid treatment in Arabidopsis. Plant Mol Biol **59:** 927–944

Breitenbach HH, Wenig M, Wittek F, Jordá L, Maldonado-Alconada AM, Sarioglu H, Colby T, Knappe C, Bichlmeier M, Pabst E, et al (2014) Contrasting roles of the apoplastic aspartyl protease APOPLASTIC, ENHANCED DISEASE SUSCEPTIBILITY1-DEPENDENT1 and LEGUME LECTIN-LIKE PROTEIN1 in Arabidopsis systemic acquired resistance. Plant Physiol **165:** 791–809

Brodersen P, Petersen M, Bjørn Nielsen H, Zhu S, Newman MA, Shokat KM, Rietz S, Parker J, Mundy J (2006) Arabidopsis MAP kinase4 regulates salicylic acid- and jasmonic acid/ethylene-dependent responses via EDS1 and PAD4. Plant J **47:** 532–546

Campos BM, Sforça ML, Ambrosio ALB, Domingues MN, Brasil de Souza TdeA, Barbosa JA, Paes Leme AF, Perez CA, Whittaker SB, Murakami MT, et al (2013) A redox 2-Cys mechanism regulates the catalytic activity of divergent cyclophilins. Plant Physiol **162:** 1311–1323

Century KS, Holub EB, Staskawicz BJ (1995) NDR1, a locus of *Arabidopsis thaliana* that is required for disease resistance to both a bacterial and a fungal pathogen. Proc Natl Acad Sci USA **92:** 6597–6601

Chan KX, Mabbitt PD, Phua SY, Mueller JW, Nisar N, Gigolashvili T, Stroeher E, Grassl J, Arlt W, Estavillo GM, et al (2016) Sensing and signaling of oxidative stress in chloroplasts by inactivation of the SAL1 phosphoadenosine phosphatase. Proc Natl Acad Sci USA **113:** E4567–E4576

Coaker G, Falick A, Staskawicz B (2005) Activation of a phytopathogenic bacterial effector protein by a eukaryotic cyclophilin. Science **308:** 548–550

Conte ML, Carroll KS (2013) The redox biochemistry of protein sulfenylation and sulfinylation. J Biol Chem **288:** 26480-26488

Conway JR, Lex A, Gehlenborg N (2017) UpSetR: An R package for the visualization of intersecting sets and their properties. Bioinformatics **33:** 2938–2940

Couturier J, Chibani K, Jacquot J-P, Rouhier N (2013) Cysteine-based redox regulation and signaling in plants. Front Plant Sci **4:** 105

Dai S, Schwendtmayer C, Schürmann P, Ramaswamy S, Eklund H (2000) Redox signaling in chloroplasts: Cleavage of disulfides by an iron-sulfur cluster. Science **287:** 655–658

Dixon DP, Skipsey M, Grundy NM, Edwards R (2005) Stress-induced protein s-glutathionylation in Arabidopsis. Plant Physiol **138:** 2233–2244

Domingo C, Saurí A, Mansilla E, Conejero V, Vera P (1999) Identification of a novel peptide motif that mediates cross-linking of proteins to cell walls. Plant J **20:** 563–570

Dong M, Bian Y, Dong J, Wang K, Liu Z, Qin H, Ye M, Zou H (2015) Selective enrichment of cysteine-containing phosphopeptides for subphosphoproteome analysis. J Proteome Res **14:** 5341–5347

Dubé L, Pingali P, Webb P (2012) Paths of convergence for agriculture, health, and wealth. Proc Natl Acad Sci USA **109:** 12294–12301

Durner J, Klessig DF (1996) Salicylic acid is a modulator of tobacco and mammalian catalases. J Biol Chem **271:** 28492–28501

Fernandes PA, Ramos MJ (2004) Theoretical insights into the mechanism for thiol/disulfide exchange. Chemistry **10:** 257–266

Forrester MT, Thompson JW, Foster MW, Nogueira L, Moseley MA, Stamler JS (2009) Proteomic analysis of s-nitrosylation and denitrosylation by resin-assisted capture. Nat Biotechnol **27:** 557–559

Foyer CH, Noctor G (2016) Stress-triggered redox signalling: What's in pROSpect? Plant Cell Environ **39:** 951–964

Fu ZQ, Yan S, Saleh A, Wang W, Ruble J, Oka N, Mohan R, Spoel SH, Tada Y, Zheng N, et al (2012) NPR3 and NPR4 are receptors for the immune signal salicylic acid in plants. Nature **486:** 228–232

Golumbeanu M, Beerenwinkel N (2018) Clustering time series gene expression data with TMixClust. https://www.bioconductor.org/packages/devel/bioc/vignettes/TMixClust/inst/doc/TMixClust.pdf Accessed December 14, 2018

Guo J, Gaffrey MJ, Su D, Liu T, Camp II DG, Smith RD, Qian WJ (2014a) Resin-assisted enrichment of thiols as a general strategy for proteomic profiling of cysteine-based reversible modifications. Nat Protoc **9:** 64–75

Guo J, Nguyen AY, Dai Z, Su D, Gaffrey MJ, Moore RJ, Jacobs JM, Monroe ME, Smith RD, Koppenaal DW, et al (2014b) Proteome-wide light/dark modulation of thiol oxidation in cyanobacteria revealed by quantitative site-specific redox proteomics. Mol Cell Proteomics **13:** 3270–3285

Han, Y., S. Chaouch, A. Mhamdi, G. Queval, B. Zechmann, and G. Noctor (2013). Functional analysis of Arabidopsis mutants points to novel roles for glutathione in coupling H_2O_2 to activation of salicylic acid accumulation and signaling. Antioxid Redox Signal **18:** 2106–2121.

Hansen RE, Winther JR (2009) An introduction to methods for analyzing thiols and disulfides: Reactions, reagents, and practical considerations. Anal Biochem **394:** 147–158

Holt III BF, Belkhadir Y, Dangl JL (2005) Antagonistic control of disease resistance protein stability in the plant immune system. Science **309:** 929–932

Huang LJ, Law JN, Murali TM (2018) Automating the PathLinker app for Cytoscape. F1000 Res **7:** 727

Jang J-C, León P, Zhou L, Sheen J (1997) Hexokinase as a sugar sensor in higher plants. Plant Cell **9:** 5–19

Job C, Rajjou L, Lovigny Y, Belghazi M, Job D (2005) Patterns of protein oxidation in Arabidopsis seeds and during germination. Plant Physiol **138:** 790–802

Kadota Y, Amigues B, Ducassou L, Madaoui H, Ochsenbein F, Guerois R, Shirasu K (2008) Structural and functional analysis of SGT1-HSP90 core complex required for innate immunity in plants. EMBO Rep **9:** 1209–1215

Käll L, Canterbury JD, Weston J, Noble WS, MacCoss MJ (2007) Semi-supervised learning for peptide identification from shotgun proteomics datasets. Nat Methods **4:** 923–925

Kangasjärvi S, Tikkanen M, Durian G, Aro E-M (2014) Photosynthetic light reactions—an adjustable hub in basic production and plant immunity signaling. Plant Physiol Biochem **81:** 128–134

Katagiri F, Thilmony R, He SY (2002) The *Arabidopsis thaliana–Pseudomonas syringae* interaction. Arabidopsis Book **1:** e0039

Kmiec B, Teixeira PF, Berntsson RP-A, Murcha MW, Branca RM, Radomiljac JD, Regberg J, Svensson LM, Bakali A, Langel U, et al (2013) Organellar oligopeptidase (OOP) provides a complementary pathway for targeting peptide degradation in mitochondria and chloroplasts. Proc Natl Acad Sci USA **110:** E3761–E3769

Kobayashi K, Mochizuki N, Yoshimura N, Motohashi K, Hisabori T, Masuda T (2008) Functional analysis of *Arabidopsis thaliana* isoforms of the Mg-chelatase CHLI subunit. Photochem Photobiol Sci **7:** 1188–1195

Li J, Brader G, Palva ET (2008) Kunitz trypsin inhibitor: An antagonist of cell death triggered by phytopathogens and fumonisin b1 in Arabidopsis. Mol Plant **1:** 482–495

Lindermayr C, Saalbach G, Durner J (2005) Proteomic identification of s-nitrosylated proteins in Arabidopsis. Plant Physiol **137:** 921–930

Liu P, Zhang H, Wang H, Xia Y (2014) Identification of redox-sensitive cysteines in the Arabidopsis proteome using OxiTRAQ, a quantitative redox proteomics method. Proteomics **14:** 750–762

Marchand C, Le Maréchal P, Meyer Y, Decottignies P (2006) Comparative proteomic approaches for the isolation of proteins interacting with thioredoxin. Proteomics **6:** 6528–6537

Marty L, Siala W, Schwarzländer M, Fricker MD, Wirtz M, Sweetlove LJ, Meyer Y, Meyer AJ, Reichheld J-P, Hell R (2009) The NADPH-dependent thioredoxin system constitutes a functional backup for cytosolic glutathione reductase in Arabidopsis. Proc Natl Acad Sci USA **106:** 9109–9114

Moreau M, Westlake T, Zampogna G, Popescu G, Tian M, Noutsos C, Popescu S (2013) The Arabidopsis oligopeptidases TOP1 and TOP2 are salicylic acid targets that modulate SA-mediated signaling and the immune response. Plant J **76:** 603–614

Mou Z, Fan W, Dong X (2003) Inducers of plant systemic acquired resistance regulate NPR1 function through redox changes. Cell **113:** 935–944

Muthuramalingam M, Matros A, Scheibe R, Mock H-P, Dietz K-J (2013) The hydrogen peroxide-sensitive proteome of the chloroplast in vitro and in vivo. Front Plant Sci **4:** 54

Nakagami H, Soukupová H, Schikora A, Zárský V, Hirt H (2006) A Mitogen-activated protein kinase kinase kinase mediates reactive oxygen species homeostasis in Arabidopsis. J Biol Chem **281:** 38697–38704

Nienaber L, Cave-Freeman E, Cross M, Mason L, Bailey UM, Amani P, A Davis R, Taylor P, Hofmann A (2015) Chemical probing suggests redox-regulation of the carbonic anhydrase activity of mycobacterial Rv1284. FEBS J **282:** 2708–2721

Nishimura K, van Wijk KJ (2015) Organization, function and substrates of the essential Clp protease system in plastids. Biochim Biophys Acta **1847:** 915–930

Noctor G, Foyer CH (2016) Intracellular redox compartmentation and ROS-related communication in regulation and signaling. Plant Physiol **171:** 1581–1592

Paulech J, Solis N, Edwards AV, Puckeridge M, White MY, Cordwell SJ (2013) Large-scale capture of peptides containing reversibly oxidized cysteines by thiol-disulfide exchange applied to the myocardial redox proteome. Anal Chem **85:** 3774–3780

Phipson B, Lee S, Majewski IJ, Alexander WS, Smyth GK (2016) Robust hyperparameter estimation protects against hypervariable genes and improves power to detect differential expression. Ann Appl Stat **10:** 946–963

Polge C, Jaquinod M, Holzer F, Bourguignon J, Walling L, Brouquisse R (2009) Evidence for the existence in *Arabidopsis thaliana* of the proteasome proteolytic pathway: Activation in response to cadmium. J Biol Chem **284:** 35412–35424

Puerto-Galán L, Pérez-Ruiz JM, Guinea M, Cejudo FJ (2015) The contribution of NADPH thioredoxin reductase C (NTRC) and sulfiredoxin to 2-Cys peroxiredoxin overoxidation in *Arabidopsis thaliana* chloroplasts. J Exp Bot **66:** 2957–2966

R Development Core Team (2018) R: A language and environment for statistical computing. R Foundation for Statistical Computing, Vienna, Austria, https://www.R-project.org/. Accessed December 14, 2018.

Ritchie ME, Phipson B, Wu D, Hu Y, Law CW, Shi W, Smyth GK (2015) *limma* powers differential expression analyses for RNA-sequencing and microarray studies. Nucleic Acids Res **43:** e47

Rojas CM, Senthil-Kumar M, Wang K, Ryu C-M, Kaundal A, Mysore KS (2012). Glycolate oxidase modulates reactive oxygen species–mediated signal transduction during nonhost resistance in *Nicotiana benthamiana* and Arabidopsis. Plant Cell **24:** 336–352

Rojas CM, Senthil-Kumar M, Tzin V, Mysore KS (2014) Regulation of primary plant metabolism during plant-pathogen interactions and its contribution to plant defense. Front Plant Sci **5:** 17

Rostkowski M, Olsson MH, Søndergaard CR, Jensen JH (2011) Graphical analysis of pH-dependent properties of proteins predicted using PROPKA. BMC Struct Biol **11:** 6

Rustérucci C, Aviv DH, Holt III BF, Dangl JL, Parker JE (2001) The disease resistance signaling components EDS1 and PAD4 are essential regulators of the cell death pathway controlled by LSD1 in Arabidopsis. Plant Cell **13:** 2211–2224

Sels J, Mathys J, De Coninck BM, Cammue BP, De Bolle MF (2008) Plant pathogenesis-related (PR) proteins: A focus on PR peptides. Plant Physiol Biochem **46:** 941–950

Senda K, Ogawa K (2004) Induction of PR-1 accumulation accompanied by runaway cell death in the lsd1 mutant of Arabidopsis is dependent on glutathione levels but independent of the redox state of glutathione. Plant Cell Physiol **45:** 1578–1585

Shapiguzov A, Edvardsson A, Vener AV (2006) Profound redox sensitivity of peptidyl-prolyl isomerase activity in Arabidopsis thylakoid lumen. FEBS Lett **580:** 3671–3676

Sharma YK, Léon J, Raskin I, Davis KR (1996) Ozone-induced responses in *Arabidopsis thaliana*: The role of salicylic acid in the accumulation of defense-related transcripts and induced resistance. Proc Natl Acad Sci USA **93:** 5099–5104

Slade WO, Werth EG, McConnell EW, Alvarez S, Hicks LM (2015) Quantifying reversible oxidation of protein thiols in photosynthetic organisms. J Am Soc Mass Spectrom **26:** 631–640

Sobotta MC, Liou W, Stöcker S, Talwar D, Oehler M, Ruppert T, Scharf AN, Dick TP (2015) Peroxiredoxin-2 and STAT3 form a redox relay for H_2O_2 signaling. Nat Chem Biol **11:** 64–70

Spoel SH, Dong X (2012) How do plants achieve immunity? Defence without specialized immune cells. Nat Rev Immunol **12:** 89–100

Spoel SH, Loake GJ (2011) Redox-based protein modifications: The missing link in plant immune signalling. Curr Opin Plant Biol **14:** 358–364

Stael S, Kmiecik P, Willems P, van der Kelen K, Coll NS, Teige M, Van Breusegem F (2015) Plant innate immunity—sunny side up? Trends Plant Sci **20:** 3–11

Ströher E, Dietz KJ (2008) The dynamic thiol-disulphide redox proteome of the *Arabidopsis thaliana* chloroplast as revealed by differential electrophoretic mobility. Physiol Plant **133:** 566–583

Suzuki N, Koussevitzky S, Mittler R, Miller G (2012) ROS and redox signalling in the response of plants to abiotic stress. Plant Cell Environ **35:** 259–270

Szklarczyk D, Morris JH, Cook H, Kuhn M, Wyder S, Simonovic M, Santos A, Doncheva NT, Roth A, Bork P, et al (2016) The STRING database in 2017: Quality-controlled protein–protein association networks, made broadly accessible. Nucleic Acids Res **45:** D362–D368

van der Hoorn RA (2008) Plant proteases: From phenotypes to molecular mechanisms. Annu Rev Plant Biol **59:** 191–223

Vercammen D, van de Cotte B, de Jaeger G, Eeckhout D, Casteels P, Vandepoele K, Vandenberghe I, Van Beeumen J, Inzé D, van Breusegem F (2004) Type II metacaspases Atmc4 and Atmc9 of *Arabidopsis thaliana* cleave substrates after arginine and lysine. J Biol Chem **279:** 45329–45336

Vizcaíno JA, Deutsch EW, Wang R, Csordas A, Reisinger F, Ríos D, Dianes JA, Sun Z, Farrah T, Bandeira N, et al (2014) ProteomeXchange provides globally coordinated proteomics data submission and dissemination. Nat Biotechnol **32:** 223–226

Wang H, Alvarez S, Hicks LM (2012a) Comprehensive comparison of iTRAQ and label-free LC-based quantitative proteomics approaches using two *Chlamydomonas reinhardtii* strains of interest for biofuels engineering. J Proteome Res **11:** 487–501

Wang H, Wang S, Lu Y, Alvarez S, Hicks LM, Ge X, Xia Y (2012b) Proteomic analysis of early-responsive redox-sensitive proteins in Arabidopsis. J Proteome Res **11:** 412–424

Wang Y-Q, Feechan A, Yun B-W, Shafiei R, Hofmann A, Taylor P, Xue P, Yang F-Q, Xie Z-S, Pallas JA, et al (2009) S-nitrosylation of AtSABP3 antagonizes the expression of plant immunity. J Biol Chem **284:** 2131–2137

Waszczak C, Akter S, Eeckhout D, Persiau G, Wahni K, Bodra N, van Molle I, De Smet B, Vertommen D, Gevaert K, et al (2014) Sulfenome mining in *Arabidopsis thaliana*. Proc Natl Acad Sci USA **111:** 11545–11550

Watanabe N, Lam E (2011) Arabidopsis metacaspase 2d is a positive mediator of cell death induced during biotic and abiotic stresses. Plant J **66:** 969–982

Westlake TJ, Ricci WA, Popescu GV, Popescu SC (2015) Dimerization and thiol sensitivity of the salicylic acid binding thimet oligopeptidases TOP1 and TOP2 define their functions in redox-sensitive cellular pathways. Front Plant Sci **6:** 327

Xiao W, Sheen J, Jang J-C (2000) The role of hexokinase in plant sugar signal transduction and growth and development. Plant Mol Biol **44:** 451–461

Yang J, Carroll KS, Liebler DC (2016) The expanding landscape of the thiol redox proteome. Mol Cell Proteomics **15:** 1–11

Yao N, Greenberg JT (2006) Arabidopsis ACCELERATED CELL DEATH2 modulates programmed cell death. Plant Cell **18:** 397–411

Yoshida K, Hisabori T (2016) Adenine nucleotide-dependent and redox-independent control of mitochondrial malate dehydrogenase activity in *Arabidopsis thaliana*. Biochim Biophys Acta **1857:** 810–818

Yoshioka-Nishimura M, Nanba D, Takaki T, Ohba C, Tsumura N, Morita N, Sakamoto H, Murata K, Yamamoto Y (2014) Quality control of photosystem II: Direct imaging of the changes in the thylakoid structure and distribution of FtsH proteases in spinach chloroplasts under light stress. Plant Cell Physiol **55:** 1255–1265

Zhang B, Tremousaygue D, Denancé N, van Esse HP, Hörger AC, Dabos P, Goffner D, Thomma BP, van der Hoorn RA, Tuominen H (2014) PIRIN2 stabilizes cysteine protease XCP2 and increases susceptibility to the vascular pathogen *Ralstonia solanacearum* in Arabidopsis. Plant J **79:** 1009–1019